

Crystallization-Induced Fluid Flow in Polymer Melts Undergoing Solidification

Donghua Xu and Zhigang Wang*

CAS Key Laboratory of Engineering Plastics,
Joint Laboratory of Polymer Science and Materials,
Institute of Chemistry, Chinese Academy of Sciences,
Beijing 100080, China

Jack F. Douglas*

Polymers Division, National Institute of Standards and
Technology, Gaithersburg, Maryland 20899

Received December 8, 2006

Revised Manuscript Received January 18, 2007

The influence of processing conditions on the morphology of solidified semicrystalline polymer materials formed under dynamic melt processing conditions has been of concern for decades.¹ Although there has been much recent progress in modeling the kinetics and origin of polymer spherulitic crystallization,^{2,3} the influence of fluid flow and the viscous properties of the undercooled polymer melt on the crystallization morphology have received relatively little attention due to the great computational problems involved in modeling and the experimental difficulties in observing this phenomenon. It is often argued that the macromolecules of the undercooled melt can diffuse to the crystal growth front during crystallization,⁴ and fluid flow processes are simply ignored. While this assumption may be a reasonable approximation under low undercooling conditions, one may well wonder whether this situation remains true under the conditions of rapid solidification that normally arise during polymer material processing. Flow in the undercooled polymer melts has not been studied much experimentally previously because of the lack of methods of sufficient temporal and spatial resolution to discriminate between the crystalline and amorphous phases during the course of the crystallization process. It is well-known, however, that the formation of commercial semicrystalline polymeric products by injection moldings, film extrusions, film blowing, etc. can be accompanied by the formation of unwanted defects (voids, pores, and other imperfections) and that the ultimate properties of these materials can be appreciably affected by processing conditions.⁵ The present study indicates that rapid fluid flow can occur in a model undercooled polymer melt (a common commercial polymer, isotactic polypropylene) during the course of crystallization under confinement conditions (simply crystallizing polymer film between cover glasses). We have also observed a similar behavior (not yet published) in crystallizing poly(ethylene oxide) (PEO) melts, indicating some degree of generality for the phenomenon.

The isotactic polypropylene (iPP) polymer employed in this work was a commercial grade polymer obtained from the Aldrich Chemical Co., and we show typical results for an isothermal crystallization temperature of 138 °C. The “weight” and “number” molecular masses M_w and M_n were about 340 000 and 97 000, respectively, so this polymer was rather polydisperse, typical of commercial material. The carbon black (CB) relative mass of the probe particles to the polymer matrix was relatively low, 0.5%. The iPP and CB were mixed by melt-

pressing repeatedly (five times) on a hot plate at 200 °C. Samples for the crystallization and flow measurements were prepared by pressing the melt mixtures between two cover glasses into thin films having a thickness of about 30 μm , thus providing a model confinement environment for the polymer melt crystallization process. Our optical microscope (Carl Zeiss JENA, made in Germany), equipped with a CCD camera (HV1301UC, made by the Da Heng Co. in Beijing), was used to image flows in the undercooled melts by following the motion of CB particles during isothermal crystallization. The resolution of the CCD camera in the x and y directions was about 0.2 μm . A homemade dual-temperature microscope hot stage provided a temperature control, with a temperature uncertainty of ± 0.1 °C. The iPP samples were first melted at 200 °C for 10 min to melt the crystallized structures formed in the course of the previous sample history and then were rapidly transferred to a crystallization temperature below the melting temperature (160 °C). Figure 1 shows a serial of micrographs of the iPP sample during isothermal crystallization at 138 °C. The present work not only considers the standard problem of characterizing the spherulite growth, but also considers how spherulite growth induces flow in the surrounding polymer melt by observing the motion trajectories of CB particles in the undercooled iPP “melt”. The basic concept of our measurement can be understood from the following nautical analogy: The undercooled melt can be viewed as a sea and the growing spherulites as islands that grow up out of this sea. The CB particles are convected by the fluids, providing information about the prevailing local “currents” in the undercooled polymer melt.

In Figure 1, the positions of three representative CB particles are marked to show their positions at a particular time in the course of iPP spherulitic crystallization. Note that bright field images were obtained, rather than the cross-polarized field images, because we are mostly interested in monitoring the positions of CB particles during the course of the crystallization process. It is apparent that while most of the iPP nuclei appear after about 14 min, the CB particles do not show any obvious movements at the spatial resolution of our optical microscope (≈ 1 μm). This is expected since the viscosity of the undercooled polymer melt is relatively large. It is also probably true that the spherulites have a relatively sparse branched internal structure at this early stage of growth and that these structures become more space-filling at longer time where secondary crystallization occurs on the early stage growth structure, resulting in further local densification.⁶ We see that the CB particles begin to move at an appreciable rate after about 24 min (the sizes of the nearby spherulites are about 30–40 μm). This CB particle motion becomes more and more rapid until the spherulites form a *percolating structure* so that the moving CB particles are surrounded by impinging spherulites. At this point, the particle movement and fluid flow become sharply attenuated. The spherulite centers remain stationary throughout the measurement to within measurement uncertainty.

Figure 2 displays the trajectories of the three CB particles marked in Figure 1. For convenience, we simply take the coordinates of original locations of the three CB particles as (0, 0). It can be seen from Figure 2 that the three CB particles all move, but they move different distances and directions depending on their local environments with respect to the growing spherulites. The flow is not caused by temperature gradients from the experimental setup because in that case the

* Corresponding authors. E-mail: zgwang@iccas.ac.cn; jack.douglas@nist.gov.

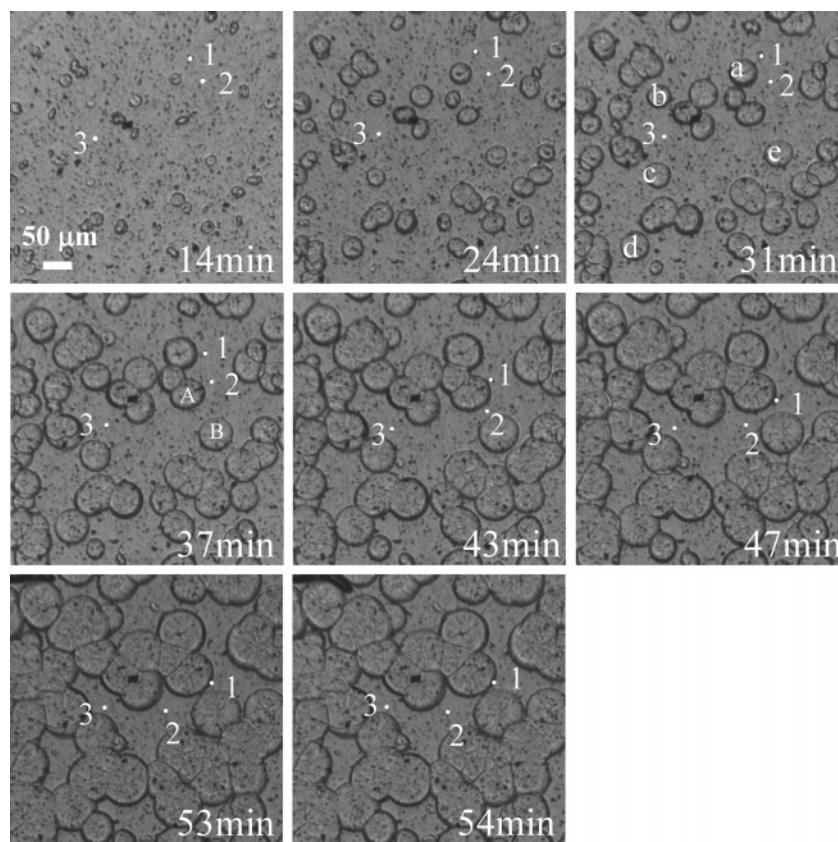


Figure 1. Selected optical micrographs of isotactic polypropylene filled with CB particles during isothermal crystallization at 138 °C. The numbers 1, 2, and 3 correspond to three representative CB particles, whose movements reflect flow of the undercooled polymer melt. The CB particles are marked by white spots for clarity. The spherulites marked as a, b, c, d, and e in the micrograph at 31 min were chosen to calculate the radial growth rates of the spherulites. The marked spherulites A and B in the micrograph at 37 min indicate a region of a strait-like flow channel.

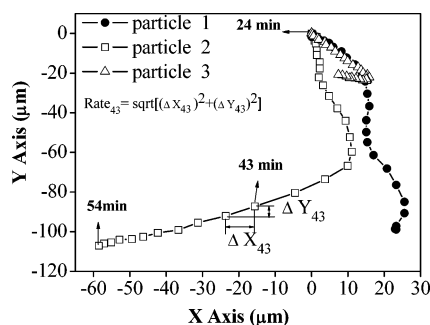


Figure 2. Trajectories of the three CB particles in two-dimensional space. Particles 1, 2, and 3 were the same three CB particles shown in Figure 1. ΔX_{43} and ΔY_{43} are displacements of particle 2 along X- and Y-axes in a minute from the crystallization time of 43–44 min, respectively. The uncertainty of the displacement is about 3%.

flow should occur in the direction of the temperature gradient.

Since the location of CB particles inside the thickness direction (z direction) of the sample cannot be clearly defined using our optical microscope, the possible movement of CB particles along z direction could not be determined in the present measurements. Thus, the CB particles may move to some degree in the thickness direction of the sample. The CB particle positions relative to the glass surfaces may also affect their velocity. Nonetheless, even though we neglect these effects, the flow velocity in the x – y plane alone is still significant, and we focus on this phenomenon to obtain an initial qualitative understanding of crystallization-induced flow.

From Figure 2, we can calculate the average displacement rate of the CB particles by taking the averaged displacement after minute intervals, and our findings are indicated in Figure

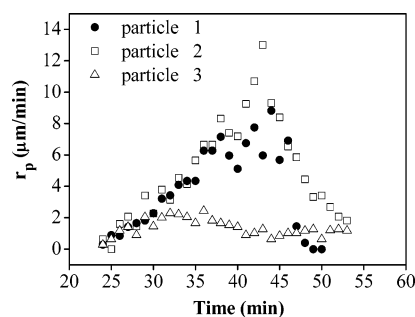


Figure 3. Displacement rates of the three CB particles during crystallization of isotactic polypropylene at 138 °C. Particles 1, 2, and 3 were the same three CB particles shown in Figure 1. The uncertainty of the displacement rate is about 3%.

3. We see that the particle displacement rate for each particle shows a sharp maximum near the time when the geometrical percolation of the spherulites occurs. The average displacement rates (local flow velocities) for the fastest three particles are 9, 13, and 2 $\mu\text{m}/\text{min}$. Clearly, particle 2 has the largest displacement rate of these three particles, with the displacement rate reaching a peak at about 43 min, close to the time where a spanning cluster of spherulites first occurs. Particle 3, on the other hand, moves the shortest distance and exhibits a much smaller average displacement rate. We can understand this variation from the local environments sensed by these particles. Particle 3 is constrained to a region surrounded by a group of spherulites from an early time in the growth process. Consider the strait-like channel between the marked spherulites A and B (see 37 min micrograph in Figure 1). After 43 min, particle 2 just squeezes through this strait before it closes, while particle 1 does not escape entrapment. The highest particle displacement

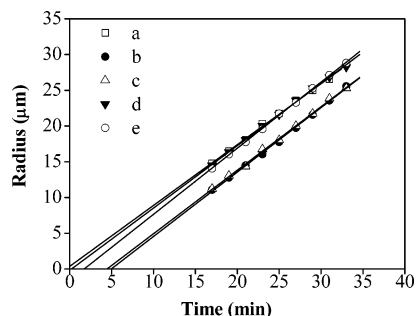


Figure 4. Time evolution of the radii of the selected five spherulites of isotactic polypropylene during isothermal crystallization at 138 °C. The locations of these spherulites are marked as a, b, c, d, and e in the micrograph at 31 min in Figure 1. The slopes of the solid lines indicate the similar growth rates of these spherulites. The uncertainty of the radius is about 1%.

rate for particle 2 corresponds to the time regime where the strait is beginning to pinch off. There are many regions that become disconnected at the same time as the spherulites percolate and the flow in these disconnected regions then drops precipitously.

From the growth curves of the spherulite radii shown in Figure 4, we estimate an average spherulite growth rate of 0.86 $\mu\text{m}/\text{min}$ over a time interval from ≈ 17 to 33 min. Evidently, the flow of the undercooled melt, which starts at about 24 min, does not cause a detectable change in the spherulite growth rate. It seems remarkable that the particle displacement rate in the undercooled polymer melt is faster than the spherulite growth rate.

These observations of particle movement naturally lead to questions about how the flow is generated during crystallization. First, we must consider the possible influence of the weight of the cover glass. In some cases, such as in polymer melts with low viscosity, the weight of the cover glass can itself induce flow in the fluid as it settles toward the other slip under gravity. However, we did not observe any movements of CB particles for samples above the melting temperature (170 °C) for 2 h with the cover glass on the top surface. Because the polymer fluid at 138 °C has a much higher viscosity than at 170 °C, we conclude that cover-slip settling does not induce fluid flow in our measurements.

Then, we considered the possible influence of exclusion and segregation of the amorphous polymer components on the movement of CB particles during the course of crystallization. It is well-known that for semicrystalline polymer/amorphous polymer or semicrystalline polymer/inorganic particles systems the amorphous polymer components or inorganic particles can segregate to the crystal growth front.^{7,8} For the iPP polymer melt, we suggest that this process occurs so that some fraction of the iPP material (the “amorphous” component) is unable to crystallize during the primary crystal growth regime, and this material then forms a viscous undercooled matrix surrounding the crystallized domains. This amorphous material later crystallizes, accounting for “secondary crystallization”, or solidifies into a vitreous state, accounting for the semicrystalline nature of these complex materials. Since this material rejection process is expected to be prevalent at the spherulite growth boundary, it is possible that the growing spherulites directly exert a repulsive force on the CB particles. Such a force would be expected to be strongly dependent on the minimum distance between the grouped spherulites and the probing particle, a smaller distance corresponding to a larger repulsive interaction, and so we checked this possibility. The minimum distance (L) between the mass center of the grouped spherulites and that of

the probing particle can be easily measured from Figure 1. We roughly estimate this force by considering it to follow an inverse relation to L (corresponding to a lubrication force hydrodynamic interaction between the solid spherulite boundary and the particle), but this exercise does not indicate any evident correlation (see Supporting Information⁹) between L and the particle displacement rates shown in Figure 3. Evidently, particle movement does not arise from a direct repulsion of the particle from the advancing crystallization front of the spherulites.

We next explored the role of stresses in the polymer melt that arise from the volume changes that accompany local crystallization.^{10–12} Crystallization creates not only dense ordered regions of positive stress, but also relatively low-density regions (as evidenced by cavitation and the emission of large acoustic pulses in previous measurements on similar materials¹³) having a large local negative hydrostatic pressure,^{9–11} and the relaxation of these stress inhomogeneities can induce fluid flow. (Using our nautical analogy this effect is somewhat akin to the local flow created by a sinking ship where the fluid rushes in to fill the gap at the fluid surface as the ship submerges.) Since the crystallization centers occur more or less at random within the film, the resulting flow patterns that these crystal structures create are rather complex [“turbulent” in the colloquial sense, although the Reynolds number (Re) and Weissenberg number (Wi) are estimated to be quite small;⁹ $Re \sim O(10^{-15})$ and $Wi \sim O(10^{-3})$]. Galeski and co-workers have shown that the local negative hydrostatic pressures in iPP crystallization can reach values between 11 and 18 MPa¹⁴ before the melt cavitates, so that these crystallization-induced forces can be impressively large. Evidently, the forces induced by volume contraction within the fluid as crystallization occurs provide a likely explanation of the fluid flow observed in our measurements.

This interpretation of the driving force for fluid flow is readily tested by simply removing the confinement condition (confinement between cover glasses), since the local stresses can then simply relax at the free polymer surface. For such thin films with free boundaries, film thinning occurs instead of a building up of local negative pressure regions within the film as crystallization occurs.¹⁵ To check for this effect, we performed a control measurement on an iPP polymer film without an upper cover glass. Under these conditions, the CB particles remained nearly stationary throughout the crystallization process.⁹ This strongly implicates the negative hydrostatic pressure effect as the origin of the generation of the crystallization-induced fluid flow. Along the same lines, Galeski and co-workers¹² have previously shown that the emission of acoustic pulses due to cavitation within films confined between glass plates could be arrested by removing the upper cover glass.

We find that fluid flow initiates only after the degree of crystallization (X_s) reaches about 22% (X_s was estimated as the fractional area occupied by spherulites in the entire optical micrograph⁹), so that the local pressure buildup at early times is evidently insufficient to create appreciable flow. These observations strongly suggest that the partially crystallized polymer melt should be considered to be a nonequilibrium “gel” at short times where $X_s \sim O(1\%)$,¹⁶ but the buildup of stresses arising from the spherulite growth causes this weak physical gel to “yield” at later times to form a highly heterogeneous shear thinning fluid in which the fluidized regions stream within channels created by the growing spherulite regions that remain solidified. At later times, the spherulites impinge on each other and fluid flow becomes arrested and a solidified state apparently reemerges. (This transition has not been examined in viscoelastic measurements, however.) If we formally express the shear rate

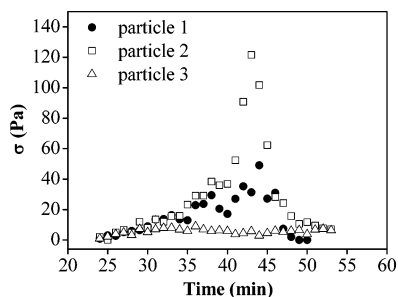


Figure 5. Changes of shear stress on the undercooled melts with crystallization time associated with the three CB probing particles in the undercooled melts. Particles 1, 2, and 3 correspond to the melt regions in which they reside. The uncertainty of the shear stress is about 2%.

as $\dot{\gamma} = V/d$, where V is the flowing rate of the undercooled melt and d is channel width, then the shear stress can be expressed as $\sigma = \dot{\gamma}\eta$ where the zero shear iPP viscosity η is on the order of 10^4 Pa·s at the temperature of our measurement. This estimate of the shear stress developing during crystallization is shown in Figure 5. We see that the maximum estimated shear stress becomes on the order $O(100$ Pa), a value much smaller than the large negative hydrostatic pressures expected to arise in confined crystallization for cavitation, $O(11\text{--}18$ MPa).¹⁴ If we adopt the estimate of 11–18 MPa from ref 14 for the magnitude of the local negative pressure (P) and identify this magnitude with the shear stress (σ), along with an order of magnitude viscosity estimate (10^4 Pa·s) at the shear stress of 10^6 Pa, we then estimate that the local shear rate $\dot{\gamma}$ should have the order magnitude, $\dot{\gamma} \sim O(100$ s⁻¹), which is sufficient for significant shear thinning. We infer from this that the induced fluid flow provides an effective means for the fluid to release the large stresses induced by local crystallization, thereby avoiding cavitation. From this observation, we might expect that both cavitation and film fracture should only occur after the spherulite percolation time because the suppression of fluid flow no longer allows for relaxation through flow. This expectation is supported by the observations of ref 14, which indicate that cavitation only starts after the crystallization half-time. The implications of spherulite percolation on cavitation, morphology, and the resulting properties of cast semicrystalline polymer materials clearly require further investigation since the phenomenon seems to be quite relevant to the resulting material properties.

We thus have the following qualitative picture of the flow processes that arise in conjunction with crystallization under confinement conditions. At an early stage of crystallization, where the spherulites form relatively “open” or “diffuse” branched structures (proceeding secondary crystallization which fills in these structures into a more compact mass), the local volume changes can be expected to be relatively modest, and thus the local negative hydrostatic pressure should be insufficient to induce substantial flow in the gel-like undercooled partially crystallized polymer “melt”. The local negative pressure builds during crystallization and at some point exceeds the yield stress and the fluid then starts to flow, thus releasing some of the stress induced by crystallization. This crystallization-induced flow accelerates until the spherulites form a geometrically percolating structure that creates a strong resistance to fluid flow, and the CB particle displacement drops off rapidly after this point so that the average particle velocity exhibits a sharp maximum.

It should be possible to inhibit fluid flow through the formation of networks of filler particles. (Carbon nanotubes^{17,18} or clay particles can likewise inhibit fluid flow through the formation of a percolating network within the polymer matrix.)

Recent work¹⁹ has shown that such extended particles can also dramatically influence the rate of crystal nucleation, providing another mechanism for strongly influencing the crystallization morphology. At any rate, these additives could provide a useful strategy for modifying the properties of injection-molded thermoplastics through the modification of the morphology associated with fluid flow induced by crystallization and particle-induced nucleation. We note that the addition of this type of additive up to a point where fluid flow is largely suppressed could have an unwanted effect—the buildup of large residual stresses in the polymer material could compromise the fracture and toughness characteristics of the resulting polymer nanocomposites. Consistent with this concern, we and others have observed that nanocomposites formed from iPP and carbon nanotubes, above the nanotube percolation concentration where a nanotube network interpenetrates the polymer matrix,¹⁷ are generally *highly brittle* so that these materials readily break under handling. Another factor that needs to be considered is the existence of thermal gradients across the polymer melt which can bias the nucleation and growth of the spherulites and alter the time where spherulite percolation occurs. Since such gradients often exist under real processing conditions, the effects of these gradients on the nature of crystallization-induced flow requires serious attention from both experimental and theoretical standpoints. In summary, our current exploratory study suggests that fluid flow in confined crystallizing melts is a factor that deserves further consideration for it might strongly impact the properties of commercially fabricated polymer materials.

Acknowledgment. Z.G. Wang acknowledges the financial support from “Hundred Young Talents” Program of Chinese Academy of Sciences and the National Science Foundation of China with Grants 10590355 and 20674092.

Supporting Information Available: Estimates of Re , Wi , and apparent crystallinity (X_s) and indication of weak correlation between the melt flow and the repulsion of the particles from the crystal growth fronts. This material is available free of charge via the Internet at <http://pubs.acs.org>.

References and Notes

- (1) Lauritzen, J. I.; Hoffman, J. D. *J. Appl. Phys.* **1973**, *44*, 4340.
- (2) Gránásy, L.; Pusztai, T.; Börzsönyi, T.; Warren, J. A.; Douglas, J. F. *Nat. Mater.* **2004**, *3*, 645.
- (3) Gránásy, L.; Pusztai, T.; Tegze, G.; Warren, J. A.; Douglas, J. F. *Phys. Rev. E* **2005**, *72*, 011605.
- (4) Mullin, J. W., Eds. *Crystallization*; Butterworth-Heinemann: Oxford, 2000.
- (5) Tadmor, Z.; Gogos, C. G. *Principles of Polymer Processing*; John Wiley & Sons: New York, 1979.
- (6) Hsiao, B. S.; Wang, Z. G.; Yeh, F.; Gao, Y.; Sheth, K. C. *Polymer* **1999**, *40*, 3515.
- (7) Chen, H. L.; Li, L. J.; Lin, T. L. *Macromolecules* **1998**, *31*, 2255.
- (8) Maiti, P.; Nam, P. H.; Okamoto, M.; Hasegawa, N.; Usuki, A. *Macromolecules* **2002**, *35*, 2042.
- (9) Supporting material is available online.
- (10) Galeski, A.; Piorkowska, E. *J. Polym. Sci., Part B* **1983**, *21*, 1299.
- (11) Galeski, A.; Piorkowska, E. *J. Polym. Sci., Part B* **1990**, *28*, 1171.
- (12) Pawlak, A.; Galeski, A. *J. Polym. Sci., Part B* **1990**, *28*, 1813.
- (13) Galeski, A.; Koenczoel, L.; Piorkowska, E.; Baer, E. *Nature (London)* **1986**, *325*, 40.
- (14) Piorkowska, E.; Galeski, A. *J. Polym. Sci., Part B* **1993**, *31*, 1285.
- (15) Nowacki, R.; Kolasinska, J.; Piorkowska, E. *J. Appl. Polym. Sci.* **2001**, *79*, 2439.
- (16) Elmoumni, A.; Winter, H. H.; Waddon, A. J. *Macromolecules* **2003**, *36*, 6453.
- (17) Kharchenko, S. B.; Douglas, J. F.; Obrzut, J.; Grulke, E. A.; Migler, K. B. *Nat. Mater.* **2004**, *3*, 564.
- (18) Kashiwagi, T.; Grulke, E.; Hilding, J.; Groth, K.; Harris, R.; Butler, K.; Shields, J.; Kharchenko, S.; Douglas, J. *Polymer* **2004**, *45*, 4227.
- (19) Nowacki, R.; Monasse, B.; Piorkowska, E.; Galeski, A.; Haudin, J. M. *Polymer* **2004**, *45*, 4877.